



Pattern Formation in a Generalized Chemotactic Model

M. R. MYERSCOUGH
School of Mathematics and Statistics,
F07, University of Sydney,
N.S.W. 2006, Australia

P. K. MAINI* AND K. J. PAINTER
Centre for Mathematical Biology,
Mathematical Institute,
24–29 St Giles',
Oxford OX1 3LB, U.K.

Many models have been proposed for spatial pattern formation in embryology and analyzed for the standard case of zero-flux boundary conditions. However, relatively little attention has been paid to the role of boundary conditions on the form of the final pattern. Here we investigate, numerically, the effect of nonstandard boundary conditions on a model pattern generator, which we choose to be of a cell-chemotactic type. We specifically focus on the role of boundary conditions and the effects of scale and aspect ratio, and study the spatiotemporal dynamics of pattern formation. We illustrate the properties of the model by application to the spatiotemporal sequence of skeletal development.

© 1998 Society for Mathematical Biology

1. INTRODUCTION: MATHEMATICAL MODELS FOR PATTERN FORMATION IN DEVELOPMENTAL BIOLOGY

One of the main areas of research in developmental biology seeks to understand the key processes and mechanisms that underlie the development of structure and form within an embryo. A number of mathematical models have been proposed in this context. Broadly speaking, they fall into two main classes: chemical prepattern models—in which a uniform density of cells responds to a chemical prepattern and differentiates accordingly, and cell movement models—in which the cells themselves form a spatial pattern with those cells which are in high-density aggregates differentiating.

The two main chemical prepattern models are gradient models and reaction–diffusion models. In the former, a simple gradient in some chemical concentration is set up and this is interpreted by cells which differentiate according to a complex mechanism involving multiple thresholds (Wolpert, 1969). In the latter, the complex interaction of reaction and diffusion in a system of chemicals leads to a pattern of peaks and troughs in chemical (morphogen) concentration (Turing,

*Author to whom correspondence should be addressed.

1952) which, it is hypothesized, is then ‘read off’ by cells which differentiate if the morphogen concentration lies above a certain threshold. Therefore, one of the main differences between these models is that in the former the chemical prepatterning mechanism is simple but the interpretation mechanism is complex, while the reverse is true for the latter (Nagorcka, 1989).

The two widely known examples of cell-movement models are mechanochemical models and chemotactic models. In mechanochemical models (Oster *et al.*, 1983), pattern arises as the result of cell traction exerted by mesenchymal cells on the extracellular matrix. This cell traction destabilizes the uniform steady state which results in a pattern of peaks and troughs in cell density. In chemotactic models, cells secrete a chemical (chemoattractant) and move up a gradient in this chemical. It is well known that this is a mechanism for generating spatial patterns in cell density (Keller and Segel, 1970). In cell-movement models, the pattern is in cell density and it is assumed that cells which are in high-density aggregates then differentiate (although this is not explicitly included in any of these models). Murray (1989) reviewed in detail both types of model and their application to a wide range of developmental patterning phenomena.

There are many similarities between reaction–diffusion, mechanochemical and chemotactic pattern generators. All are based on the interaction between an activating mechanism, which is promoting growth (of chemical concentration or cell density) and an inhibiting mechanism, which depresses growth. The uniform steady state is destabilized when the balance between these two mechanisms is tipped in favor of the activating mechanism due to, for example, greater diffusion of inhibitor than of activator in the case of reaction–diffusion. A spatially homogeneous steady state then evolves into a spatially heterogeneous state. This is a generalization of diffusion-driven instability, which applies specifically to reaction–diffusion systems. The linear analyzes of these models are all similar mathematically and lead to the prediction of bifurcation from spatially uniform solutions to spatially nonuniform solutions. In the vicinity of primary bifurcation points, these spatially nonuniform solutions are eigenfunctions of the Laplacian with appropriate boundary conditions on the domain. This naturally leads to the concept of developmental constraints, where certain key features of spatial patterns hold independently of the mechanism which generated them (Oster *et al.*, 1988).

Models of this form have been widely studied for the standard case of a homogeneous domain, that is, the parameters are constant across the whole domain, with zero-flux boundary conditions. Recently, however, there have been a number of papers devoted to the analysis of such models on asymmetric domains, where certain key parameters show a spatial or spatio-temporal dependence (see, for example, Hunding and Brøns, 1990; Maini *et al.*, 1992; Kulesa *et al.*, 1995). The role of generalized boundary conditions on the spatial patterns exhibited by a standard reaction diffusion model has also been analyzed by Dillon *et al.* (1993).

Here we focus on a cell chemotactic model for pattern formation. In Section 2

we briefly review previous results on general cell chemotaxis models. In Section 3 we introduce the specific model that we analyse. In subsequent sections we investigate the role of boundary conditions and the effect of scale on the patterns exhibited by the model using numerical methods. The one-dimensional results provide us with crucial insight into the behavior of the model in two dimensions, which is discussed in Section 6. A possible application to skeletal patterning in the vertebrate limb is presented in Section 7.

2. CHEMOTACTIC MODELS AND PATTERN FORMATION

Much of the recent work on chemotactic models has concentrated on waves of migrating cells or other entities in various contexts. These include angiogenesis (Chaplain and Stuart, 1993), various cell migration assays (Ford and Lauffenberger, 1991, Sherratt *et al.*, 1993), propagating patterns (Myerscough and Murray, 1992) and even herd grazing (Gueron and Liron, 1989). Rather less attention has been given to chemotactic pattern formation. The seminal work of Keller and Segel (1970) addressed the problem of pattern formation among aggregating *Dictyostelium* amoebae. More recent models for this phenomenon couple the excitable dynamics of the signaling chemical cAMP and cell receptors to the chemotactic cell response to cAMP to produce the streaming instability characteristic of *Dictyostelium* aggregation (see, for example, Höfer *et al.*, 1995a,b). Chemotactic models have also been proposed for skin pigment patterns in reptiles, specifically stripe patterns in alligators (Murray, *et al.*, 1990) and snake-skin markings (Murray and Myerscough, 1991).

The basic general chemotaxis model takes the form:

$$\frac{\partial n}{\partial t} = \nabla \cdot (D_n \nabla n) - \nabla \cdot (nf(n, c) \nabla c) + h(n, c) \quad (1)$$

$$\frac{\partial c}{\partial t} = \nabla \cdot (D_c \nabla c) + g(n, c) \quad (2)$$

where n is cell density and c is the concentration of chemoattractant; D_n and D_c are diffusion coefficients, $f(n, c)$ models the chemotactic response of the motile cells, $h(n, c)$ models cell division and cell death, and $g(n, c)$ models chemoattractant production and degradation. This type of model was first proposed by Keller and Segel (1970). Typical boundary conditions for a pattern-formation model are traditionally periodic or zero flux. The effect of different types of boundary conditions has not been addressed for this model.

The form of the function $f(n, c)$ which controls the chemotactic response of the cells to the chemoattractant ultimately depends on the sensitivity of the cells at different concentrations of the attractant. The simplest form for $f(n, c)$ is $f(n, c) = \alpha$, a constant (see, for example, Maini *et al.*, 1991; Chaplain and Stuart, 1993). This assumes that the sensitivity of cells to attractant is independent of chemoattractant concentration. If cell sensitivity to chemoattractant

concentration is known to decrease as concentration increases then one possible model is $f(n, c) = \chi/c$, where χ is constant (Keller and Segel, 1971). The action of cell-surface receptors has been modeled by setting $f(n, c) = \chi k/(k+c)^2$, where k and χ are constants (Lapidus and Schiller, 1976; Ford and Lauffenberger, 1991). The above models are phenomenological. Recently, Othmer and Stevens (1997) derived macroscopic chemotaxis equations based on microscopic rules using a random walk approach. They showed which specific assumptions of how a cell moves give rise to the types of phenomenological macroscopic models above.

The coefficient D_n that governs the random component of cell motility may depend on chemical concentration. For example, to model chemokinesis, D_n would be an increasing function of c (Sherratt *et al.*, 1993). For simplicity, however, we will assume that D_n is constant.

The function $h(n, c)$ models cell proliferation and death. If cell numbers are conserved, i.e. $h(n, c) = 0$, then in the steady state one can integrate equation (1) and show that the final steady state is periodic or consists of a single peak or half peak (Grindrod *et al.*, 1989). When $h(n, c)$ is nonzero, cell growth is usually assumed to be logistic; i.e. $h(n, c) = rn(1 - n/n_0)$, where r and n_0 are usually constants.

The production, degradation and consumption of chemoattractant are given by the function $g(n, c)$. The degradation or consumption term in $g(n, c)$ is typically linear and the production term is of the Michaelis–Menten type (see, for example, Keller and Segel, 1970; Myerscough and Murray, 1992; Maini *et al.*, 1991; Chaplain and Stuart, 1993; Sherratt *et al.*, 1993). This form of $g(n, c)$ and the chemotactic flux of cells together form the activating processes in a chemotactic pattern-formation model. This is in contrast to reaction–diffusion models where the presence of one of the chemical species activates the pattern under suitable conditions. In the next section we present the basic chemotactic model for pattern formation that we shall analyze.

3. MODEL EQUATIONS

In order to investigate the role of boundary conditions and scale effects on patterns in cell density we consider the model analyzed in Maini *et al.* (1991).

The basic two-species model is

$$\frac{\partial n}{\partial t} = \nabla \cdot (D_n \nabla n) - \nabla \cdot (n\alpha \nabla c) + rn \left(1 - \frac{n}{n_0}\right) \quad (3)$$

$$\frac{\partial c}{\partial t} = \nabla \cdot (D_c \nabla c) + \frac{vn}{n + \gamma} - \mu c \quad (4)$$

where n is cell density and c is the concentration of chemoattractant; α is the chemotactic coefficient of the motile cells, r is the linear growth rate of the cell

population, n_0 the cell density under steady-state conditions and v , γ , and μ are constants governing the rate of chemoattractant production and degradation. We will assume that D_n and D_c are positive constants.

Equations (3) and (4) can be nondimensionalized by setting

$$\begin{aligned} n^* &= \frac{n}{n_0} & c^* &= \frac{\mu}{v}c & \mathbf{x}^* &= \left(\frac{\mu}{D_c s}\right)^{\frac{1}{2}} \mathbf{x} & t^* &= \frac{\mu t}{s} \\ D &= \frac{D_n}{D_c} & r^* &= \frac{r}{\mu} & \alpha^* &= \frac{\alpha v}{\mu D_c} & \gamma^* &= \frac{\gamma}{n_0}. \end{aligned} \quad (5)$$

Dropping the asterisks, the nondimensional equations then become

$$\frac{\partial n}{\partial t} = \nabla \cdot (D \nabla n) - \nabla \cdot (n \alpha \nabla c) + s r n (1 - n) \quad (6)$$

$$\frac{\partial c}{\partial t} = \nabla \cdot (\nabla c) + s \left(\frac{n}{n + \gamma} - c \right). \quad (7)$$

Here, s is a parameter which controls spatial and temporal scale.

We apply generalized boundary conditions

$$\theta_1 \left(D \frac{\partial n}{\partial r} - n \alpha \frac{\partial c}{\partial r} \right) = (1 - \theta_1)(\theta_2 n^s - n) \quad (8)$$

$$\theta_3 \frac{\partial c}{\partial r} = (1 - \theta_3)(\theta_2 c^s - c) \quad (9)$$

where $\frac{\partial}{\partial r}$ is the normal derivative to the boundary, θ_1 , θ_2 and θ_3 are nonnegative control parameters and n^s and c^s are the nontrivial values of n and c , respectively, for which the kinetic terms vanish, i.e. $n^s = 1$, $c^s = 1/(1 + \gamma)$. With the boundary conditions in this form we can impose very general boundary conditions by varying the control parameters θ_i , where $i = 1, 2, 3$.

Using homotopy methods, Dillon *et al.* (1993) analyzed a two-chemical reaction–diffusion model in one dimension with boundary conditions of the above form. We shall investigate the effect of different boundary conditions on the chemotactic pattern. In Sections 4 and 5 we present numerical solutions to the model equations (6) and (7) with boundary conditions (8) and (9) in one spatial dimension on the domain $0 \leq x \leq 1$ using NAG solver D03PHF to obtain time-dependent solutions and the ENTWIFE finite element package (Winters, 1985) for steady-state solutions.

4. ROLE OF BOUNDARY CONDITIONS

The above model was extensively studied by Myerscough (1988) for the case of no flux boundary conditions on both n and c (i.e. when $\theta_1 = \theta_3 = 1$ in equations (8) and (9)). The model can exhibit patterns of peaks of cell density which overlie

peaks of chemoattractant concentration. Depending on the parameter values and initial conditions used, these peaks can be internal or can lie on the boundary. Although such patterns are appropriate for applications such as skin pigmentation patterns, they are not appropriate for cases in which patterns are internal to the domain, for example, in skeletal development in the limb. Here we investigate the role of alternative boundary conditions.

4.1. The role of symmetric mixed boundary conditions. We now impose mixed boundary conditions on the system of equations (6) and (7). Specifically we take $\theta_1 = 1, \theta_2 = \theta_3 = 0$ in equations (8) and (9) so that $c = 0$ on both boundaries, while n still has no flux boundary conditions. These mixed boundary conditions eliminate the boundary peaks. This can be seen in Fig. 1. The stability of these solutions can be determined either by solving the time-evolution problem or by analyzing the steady-state problem using the ENTWIFE numerical bifurcation package.

If cells are present, i.e. $n \neq 0$, then c will not be zero except at the boundary. Hence, near each boundary there is a gradient in chemoattractant c which increases away from the boundary. Cells move up this gradient and away from the boundary. This forces pattern to occur within the domain and also eliminates boundary peaks. Dillon *et al.* (1993) found that mixed boundary conditions can also internalize peaks in the standard Turing model equations.

Symmetric boundary conditions always result in a symmetric pattern in the sense that all peaks have the same amplitude. We next explore how asymmetric boundary conditions give rise to asymmetric patterns.

4.2. The role of asymmetric mixed boundary conditions. To impose asymmetric mixed boundary conditions the values of the parameter set $\{\theta_1, \theta_2, \theta_3\}$ in equations (8) and (9) must be different at $x = 0$ from those at $x = 1$. We shall investigate asymmetric boundary conditions on c . Therefore, we fix $\theta_1 = 1$ to impose zero-flux conditions on n . For c we choose $\theta_2 = \theta_3 = 0$ at $x = 0$. At $x = 1$ we set $\theta_3 = 0$ and $\theta_2 > 0$. With these parameter values we have $c(0) = 0, c(1) = \theta_2 c^s$. The solutions to equations (6) and (7) with these boundary conditions are spatially asymmetric. Furthermore, the solutions evolve in a specific temporal fashion. This temporal sequence is shown in Fig. 2. The asymmetry in the boundary conditions for c imposes an initially large gradient in c at the boundary $x = 0$. This initiates a peak in cell density near this boundary. If further peaks form, they do so in a temporal sequence from $x = 0$ to $x = 1$; that is, the first peak to form is nearer the $x = 0$ boundary provided that θ_2 is close to 1. Their amplitudes are different and their maxima do not occur in regular intervals along the domain. Thus, we have a genuine spatial asymmetry. If $c(1) > c^s$, i.e. $\theta_2 > 1$, there is an outward gradient in c at $x = 1$ initially, as c reaches c^s internally. This results in a peak in cell density on the boundary. If $c(1) < c^s$, ($\theta_2 < 1$) then there is an inward gradient in c and peaks in n do not form on the

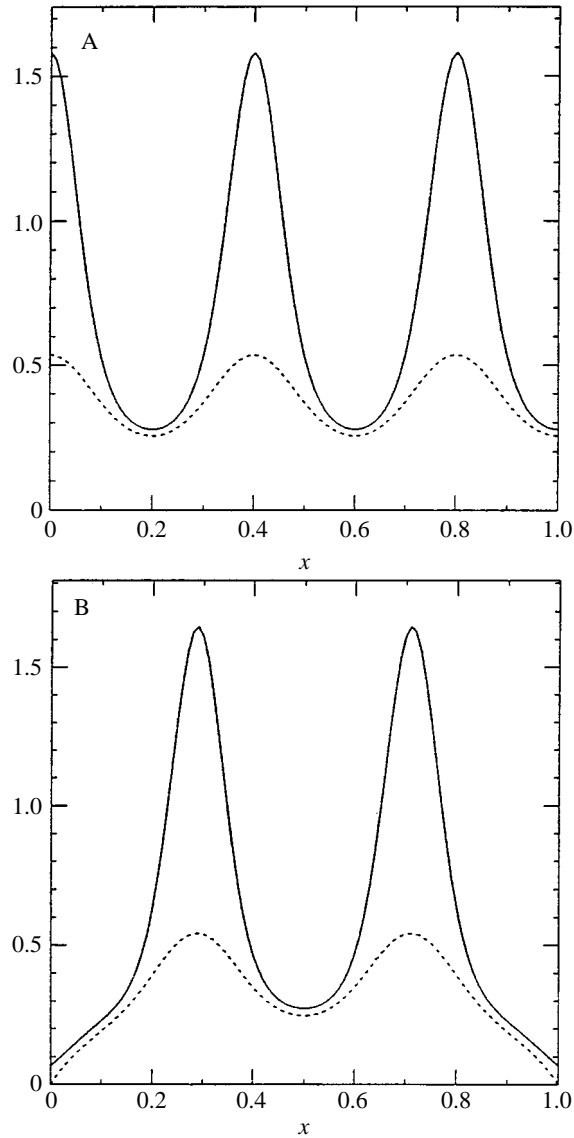


Figure 1. Numerical simulations of the cell-chemotactic model equations (6) and (7) in one dimension for different boundary conditions, with parameters $D = 0.25$, $r = 0.04$, $\alpha = 2$, $\gamma = 1$, $s = 600$. For the initial conditions we imposed random perturbations of maximum size 0.01 about the uniform state $n = 1$ for cell density, and set c to the uniform state of 0.5. The time evolution equations were solved using NAG library routine D03PHF until a steady state was reached: (a) Zero flux boundary conditions, (i.e. in equations (8) and (9) $\theta_1 = \theta_3 = 1$). (b) Mixed boundary conditions with $\theta_1 = 1$, $\theta_2 = \theta_3 = 0$ in equations (8) and (9) so that $c = 0$ on the boundary. In each case the final steady state is shown. Note that there is a boundary peak in (a), but in (b) the pattern is internalized. Note also that the pattern in (b) is 'simpler' (i.e. it has fewer peaks), than that in (a). n , —; c , - - - .

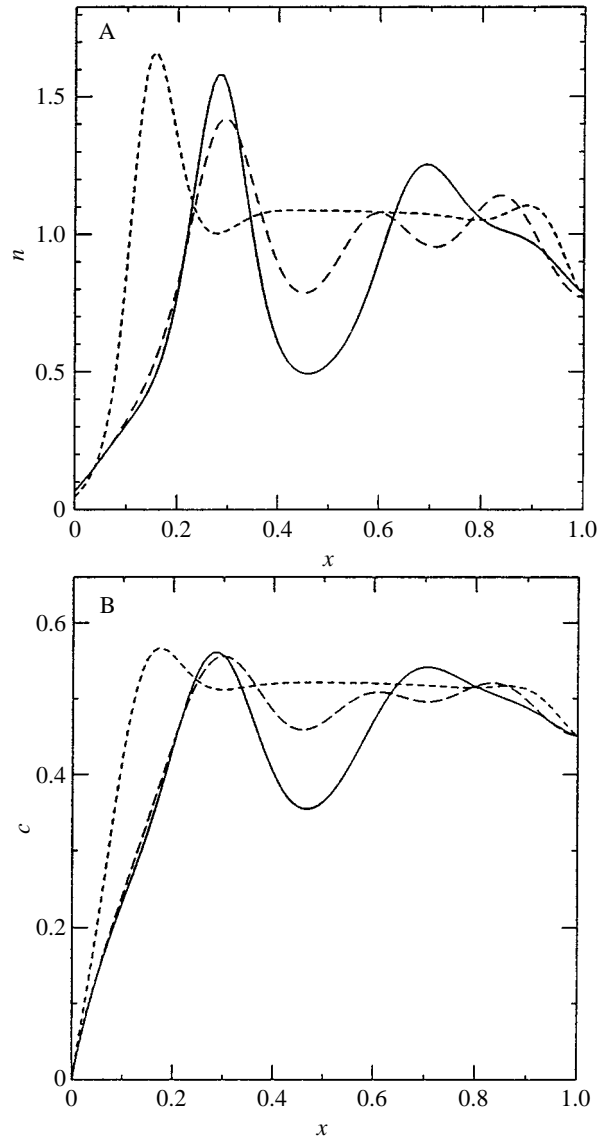


Figure 2. Time evolution for the model equations (6) and (7) in one dimension with zero flux boundary conditions on n [$\theta_1 = 1$ in equation (8)], but with asymmetric boundary conditions on c . Specifically, for the left-hand boundary $x = 0$, $\theta_2 = 0, \theta_3 = 0$ in equations (8) and (9), while for the right-hand boundary $x = 1$, $\theta_2 = 0.9, \theta_3 = 0$. With the parameters $D = 0.25, r = 0.04, \alpha = 2, \gamma = 1, s = 1000$, this corresponds to $c(0) = 0, c(1) = 0.45$. Solutions are shown for (a) cell density n , and (b) chemoattractant density c . Initial conditions as in Fig. 1. $t = 200$, ---; $t = 2000$ — — —; steady state, —.

boundary (Fig. 3). As $c(1)$ is decreased to zero the spatial asymmetry in n is lost.

5. THE EFFECTS OF SCALE

For both symmetric and asymmetric boundary conditions, the nature of the pattern, in particular the number of peaks within the pattern, will depend on the domain size, or in the non-dimensional equations (6) and (7) on the parameter s . Increasing s effectively increases the dimensional size of the domain and the dimensional evolution time.

The time-evolution problem was solved for various values of s with both symmetric and asymmetric mixed boundary conditions; a selection of these solutions are presented in Section 4. For a more comprehensive picture of how domain size influences pattern, bifurcation diagrams were generated for steady-state solutions of equations (6) and (7) in one dimension with different sets of boundary conditions. These are shown in Figs 4–7. When mixed boundary conditions are used for equations (6) and (7), no nontrivial uniform steady state exists and a nonuniform steady state always exists even for very small s . Where both n and c have no flux boundary conditions, and hence a nontrivial, uniform steady state exists, the bifurcation diagram is likely to have many branches which bifurcate from the uniform steady state (cf. Maini *et al.*, 1991; Dillon *et al.*, 1993). For mixed boundary conditions there is one unbranched curve for most values of s . In Figs 4 and 6 the measure of the steady-state solution is taken as the average of n over the domain, i.e.

$$\|n\| = \int_0^1 n(x) dx.$$

For the symmetric mixed boundary conditions of Section 4, with parameter values $D = 0.25$, $\alpha = 2$, $r = 0.04$, and $\gamma = 1$, increases in the number of peaks take place via a series of limit points. This is very different from the case in Dillon *et al.*, (1993), where transitions from one type of pattern to another can occur in the absence of a bifurcation. For example, for $s < 450$ the solution has only one peak. As s increases, this peak becomes indented at the top. This indentation deepens on rounding the limit point at $s = 544.11$ to give an unstable solution with two distinct peaks. At the next limit point, $s = 505.52$, this two-peak solution becomes stable. Thus, this fold in the bifurcation curve is associated with the formation of a minimum in n which separates the ‘split peak’ into two distinct peaks. The time-evolved solution tends to the split-peak solution which corresponds to the upper part of the fold. This is usually, but not always, the case (Figs 4 and 5).

The second fold in the bifurcation curve in Fig 4 is associated with the two-to three-peak transition. Here, the third peak begins to form in the minimum

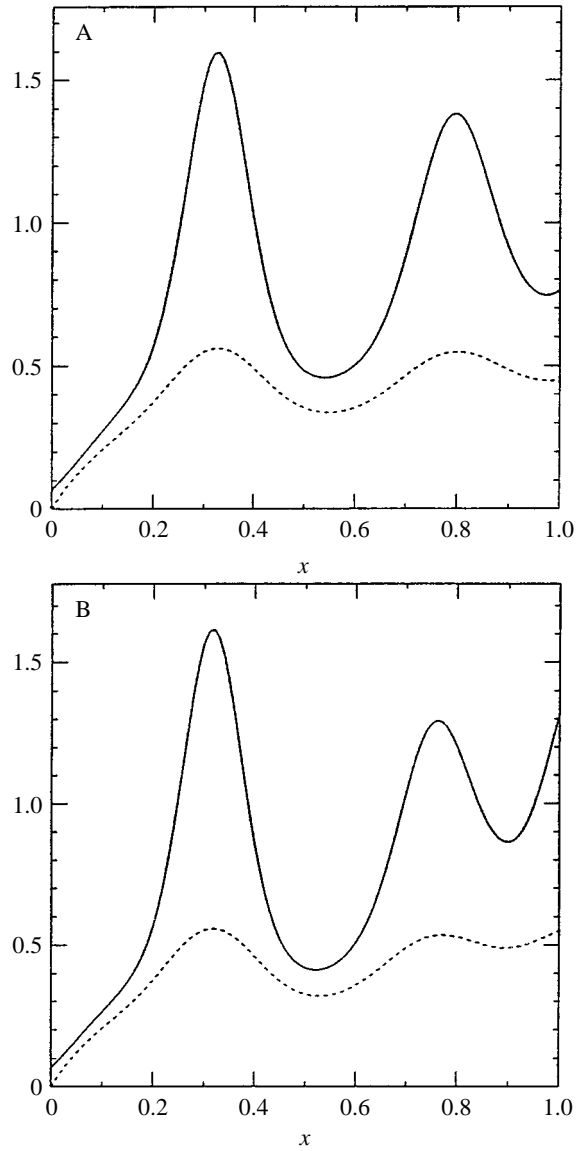


Figure 3. Steady-state solutions of equations (6) and (7) in one dimension with zero-flux boundary conditions on n [$\theta_1 = 1$ in equation (8)], but with asymmetric boundary conditions on c : $c(0)$ is kept fixed at 0 but different boundary conditions are imposed at $x = 1$: (a) $\theta_2 = 0.9, \theta_3 = 0$ in equation (9), (b) $\theta_2 = 1.1, \theta_3 = 0$ in equation (9). Parameters and initial conditions are as in Fig. 1. n , —; c , ---.

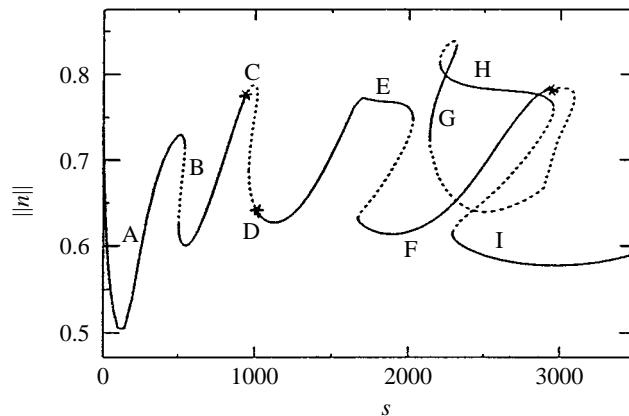


Figure 4. Bifurcation diagram for steady-state solutions of equations (6) and (7) with no flux boundary conditions on n and homogeneous Dirichlet boundary conditions on c . Parameter values used are $D = 0.25$, $\alpha = 2$, $r = 0.04$ and $\gamma = 1$.

between the existing two peaks. The formation of this peak is associated with a Hopf bifurcation in which the primary branch becomes unstable. (We will not investigate Hopf bifurcations further in this paper as our main concern is with stationary pattern.) Moving around the two limit points of this fold, the minima in n deepen to give three distinct peaks of roughly equal height.

As s increases toward the next fold, the peak in the center of the domain becomes split, and as for the first fold, this split deepens as the limit points at $s = 2028.99$ and $s = 1672.95$ are traversed to give four distinct peaks.

The bifurcation diagram becomes more complex for $s > 2000$. The next limit point, following the curve from the third fold, is close to another Hopf bifurcation which is associated with the formation of a fifth peak at the center of the domain. As before, the minima on either side of this peak deepen on rounding the limit point to give a five-peak pattern. These straightforward four- and five-peak patterns continue to be the attractors for the time-evolved solutions despite the existence of less regular patterns on other parts of the bifurcation curve between $s = 2000$ and $s = 3100$.

The bifurcation diagram for mixed asymmetric boundary conditions is shown in Fig. 6 with the corresponding steady-state solutions for n being shown in Fig. 7. There are no Hopf or secondary bifurcations for $s < 3000$ in this case. The first three folds are associated with the growth of minima in n to give new peaks. Here, because of the boundary conditions, the new peak always forms on the right-hand side of the domain where $c = 0.45$ at $x = 1$. (On the left-hand side $c = 0$ at $x = 0$.) The fourth and fifth sets of limit points, with their associated unstable regions at approximately $s = 1900$ and 2500 , are associated with a slight leftward movement of the four peaks rather than the generation of extra peaks. In this particular asymmetric case, when three solutions exist, the time-evolved solutions are attracted to the steady-state solutions on the upper part of the curve.

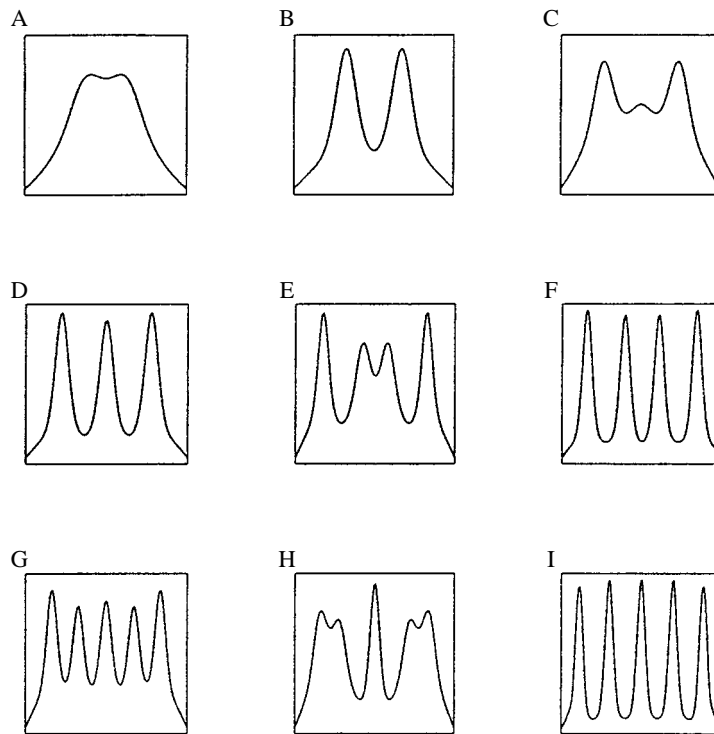


Figure 5. Steady-state solutions in n corresponding to marked points on Fig. 4 (the corresponding chemical concentration profiles are qualitatively similar to those of n).

This is not the case for every parameter set. For example, when $D = 0.35$, $\alpha = 2$, $r = 0.01$ and $\gamma = 1$, the first three folds in the bifurcation curve appear similar to those in Fig. 6. The time-evolved solutions, however, tend towards solutions on the lower part of the fold in two out of the three cases.

In this example, the case with asymmetric boundary conditions differs from the symmetric case in that the new peaks form on one side of the domain rather than at its center and there are no Hopf or secondary bifurcations. This lateral (as opposed to central) formation of new peaks in cell density, as dimensional domain size increases, distinguishes pattern formed in asymmetrical environments from pattern formed in strictly symmetrical domains.

Application of this type of model to a developmental phenomenon implicitly assumes that cells at high density differentiate so that the pattern in n exhibited by the model is the pattern observed in development. (There is evidence that in limb development, for example, cells in high-density aggregates will differentiate (see Maini and Solursh, 1991, for review).) Note that there is the possibility that transient solutions that are different from the final steady state may have an effect on the pattern of differentiated cells. However, under the biologically realistic assumption that differentiation occurs on a time scale slower than that of pattern formation, one can show that transient solutions in n have only a negligible effect

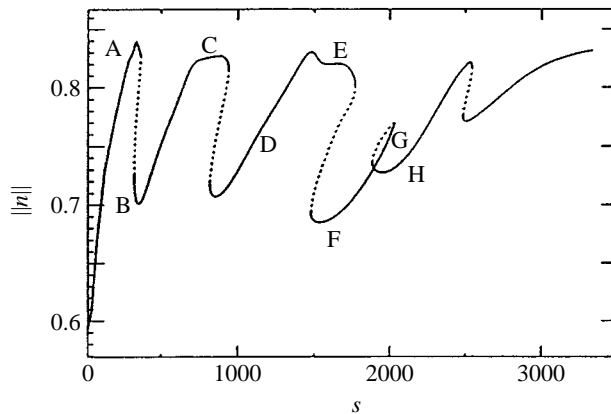


Figure 6. Bifurcation diagram for steady-state solutions of equations (6) and (7) with no flux boundary conditions on n and asymmetric boundary conditions on c ; that is, $c = 0$ at $x = 0$ and $c = 0.45$ at $x = 1$. Parameter values used are $D = 0.25$, $\alpha = 2$, $r = 0.04$ and $\gamma = 1$.

on the final solution profile of differentiated cells. Differentiation is essentially a ‘slave’ process and does not influence the qualitative form of the n and c solution profiles. Therefore, we are justified in analyzing only the steady-state problem for the $n - c$ model and then inferring the differentiated state from the n profiles.

6. TWO-DIMENSIONAL SOLUTIONS

We now consider two-dimensional domains with different types of boundary conditions. Of course, there is now much more variety in the different types of conditions that may be imposed. To investigate how the one-dimensional results generalize, we choose to focus on two types of boundary condition, which we denote by Type A and Type B (see Fig. 8). In both boundary conditions, we impose zero flux for cell density but vary the conditions for the chemical. In Type A, we have zero-flux boundary conditions along two of the boundaries and a source and sink at the other boundaries. More specifically, at the left-hand boundary we set $c = 0$ and at the right-hand boundary $c = 0.45$. For Type B, the sink extends to three of the boundaries and there is a chemical source at one end.

We define the aspect ratio a as L/W (Fig. 8), and in all the simulations presented below we fix the parameter values of D, r, γ and α as for the one-dimensional case and vary a and s . The initial conditions for the chemical concentration and cell density are set at the respective steady-state levels with a small random perturbation (1%) everywhere for the cell density.

We first consider Type A boundary conditions and investigate the extent to which stripes are maintained as we move from one to two dimensions. We find that as the parameter value s increases, stripes are maintained only if a lies above

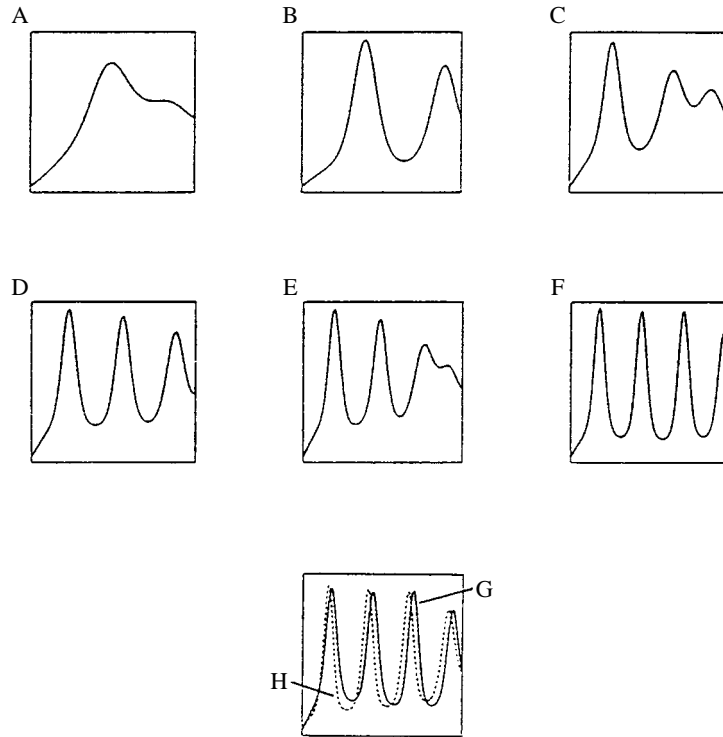


Figure 7. Steady-state solutions in n corresponding to marked points on Fig. 6.

a critical value, which can be determined from linear analysis (see Appendix). We illustrate the results in Fig. 9. Intuitively, this is as we would expect from analogy with the standard zero-flux case. In the latter, linear analysis predicts the formation of spots or stripes, depending on the parameters and initial conditions. Spots are effectively the superposition of stripes of different orientations. As a increases, the space to form multioriented stripes decreases, and at a critical value of a , stripes of only one orientation will form.

Figure 10 shows the time evolution of the pattern for the parameters $s = 900$, $a = 1$. Initially, the pattern is essentially one dimensional with three parallel stripes. This transient solution eventually breaks up into a mixed stripe/spot pattern.

The solutions for Type B boundary conditions are shown in Fig. 11 for increasing s . We increase a with s so that the domain width is kept constant. As s increases, a central spot of high-cell density splits into two spots and then a third spot emerges between these pre-existing spots.

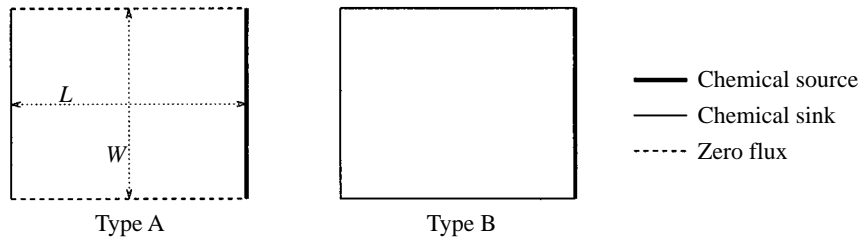


Figure 8. Schematic representation of the boundary conditions imposed on c for the two-dimensional simulations (see text for details). Boundary conditions for n are zero flux everywhere.

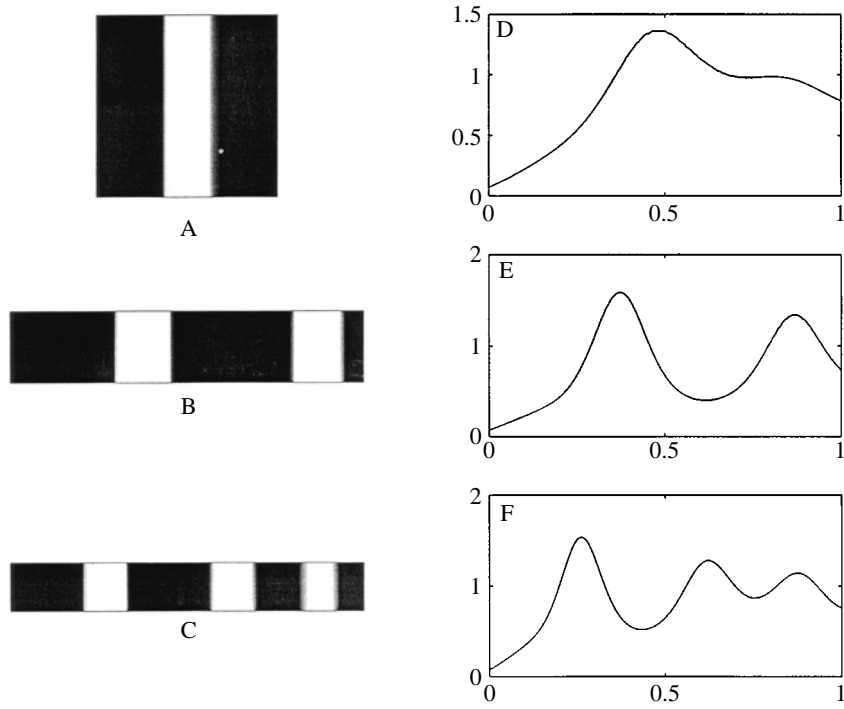


Figure 9. Steady-state solutions for n under Type A boundary conditions for varying s and a . (a) $s = 300, a = 1$; (b) $s = 400, a = 5.0$; (c) $s = 900, a = 7.41$. Corresponding one-dimensional cross sections illustrating cell density are shown in (d)–(f). [White denotes high cell density ($n > 1.1$), black denotes low cell density ($n < 1.0$)].

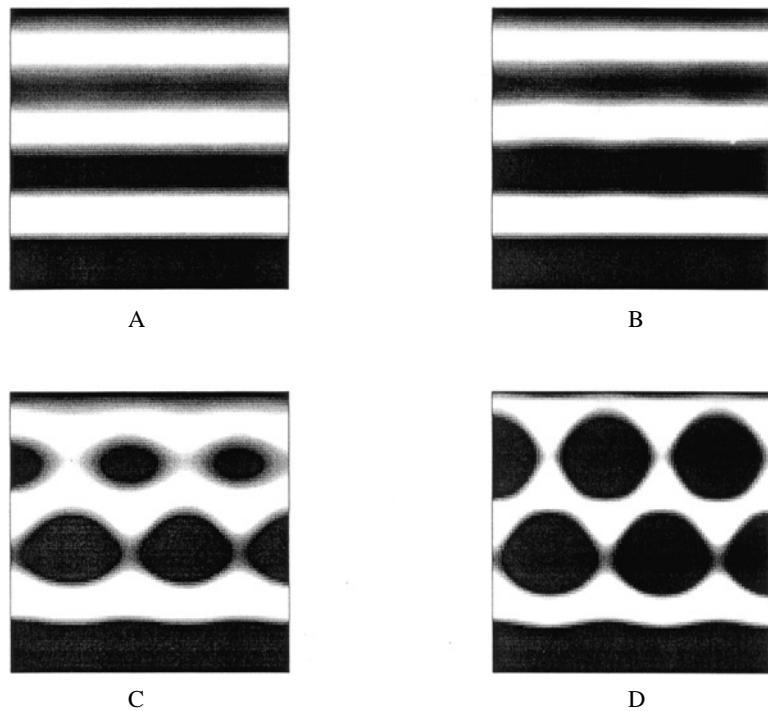


Figure 10. Time evolution for n under Type A boundary conditions for $s = 900$, $a = 1.0$. (a) $t = 0.6$, (b) $t = 1.0$, (c) $t = 2.0$, (d) $t = 4.0$. [White denotes high cell density ($n > 1.1$), black denotes low cell density ($n < 0.8$)]. Here the sink for c is at the top of each square and the source is at the bottom (that is, the figure on the left-hand side of Fig. 8 has been rotated through 90° clockwise).

7. APPLICATION TO LIMB DEVELOPMENT

Although a great deal of experimental and theoretical work has been carried out on skeletal patterning in the chick limb, several key questions remain to be answered (see Maini and Solursh, 1991, for review). Specifically, there is no theoretical model, to our knowledge, that can account for the sequence of transitions from one to two to three skeletal elements along the anterior–posterior (AP) axis of the limb, their spatial asymmetry, and the temporal sequence of their development across the AP axis. The anterior half of the limb gives rise to most of the humerus, the radius and digit II. The posterior half gives rise to the ulna and digits III and IV. The pattern is laid down in a proximo–distal (PD) and posterior–anterior sequence. For example, digit IV appears before digit III, which appears before digit II.

Bard and Lauder (1974) showed that a Turing model was unrealistic as a mechanism for digit development because of its sensitivity to initial conditions and parameter values. Newman and Frisch (1979) proposed a Turing model for skeletal development along the limb, but based their analysis on a linearized version of the model and did not fully address the role of nonlinear effects (Othmer 1986).

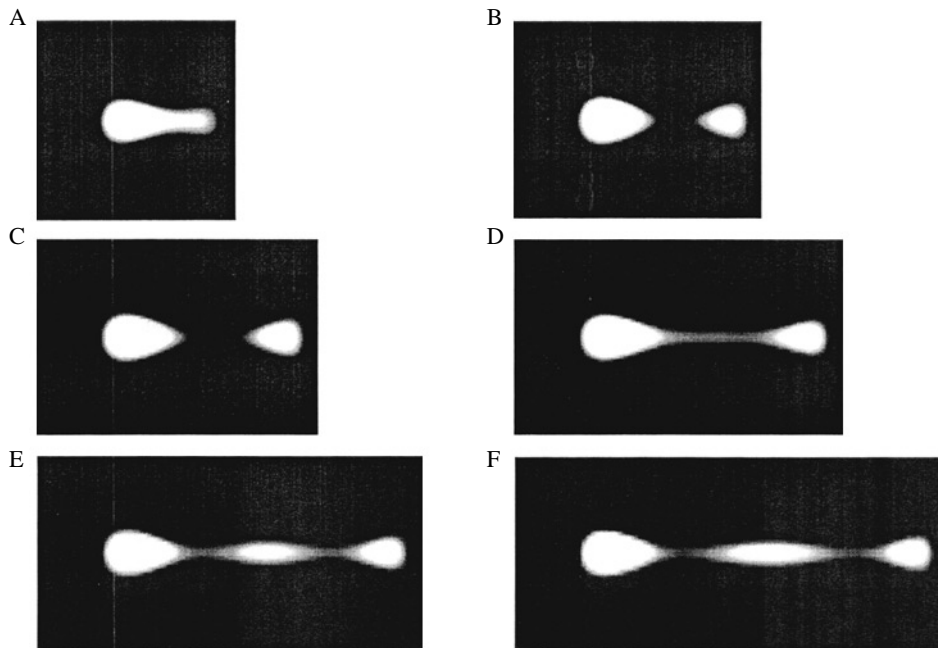


Figure 11. Steady-state solutions for n under Type B boundary conditions for varying s and a . (a) $s = 150, a = 1$; (b) $s = 225, a = 1.25$; (c) $s = 300, a = 1.43$; (d) $s = 400, a = 1.67$; (e) $s = 550, a = 1.96$; (f) $s = 700, a = 2.22$. [White denotes high cell density ($n > 1.6$), black denotes low cell density ($n < 1.4$)].

More recently, Dillon *et al.* (1993) showed that different types of boundary conditions can greatly reduce the sensitivity of patterns produced by a reaction–diffusion system, and, under appropriate boundary conditions, that the model can generate in a robust and controlled fashion the sequence of transitions from one to two to three peaks. Their model produces spatially symmetric patterns. Maini *et al.* (1992) showed that the introduction of spatial asymmetry in the diffusion coefficients of the morphogens, through a control chemical, could lead to spatial asymmetry in the solution. Such spatially asymmetric diffusion is biologically realistic (Brümmer *et al.*, 1991, Maini, 1994). Some of the models discussed above can account for the spatiotemporal sequence of pattern formation along the PD axis. At each AP cross section, however, the patterns formed by the above models arise simultaneously. This is inconsistent with the skeletal pattern in the limb which occurs in a temporal sequence across the AP axis. In fact, none of the above models addresses this issue.

In this article we have shown that spatially asymmetric boundary conditions can give rise to genuine spatio-temporal patterning. If we consider the model equations (6) and (7) in one dimension with Neumann boundary conditions on n and Dirichlet boundary conditions on c , then Figs 4–7 show that, as the domain length increases, the steady-state solution profile of cell density changes from one to two to three peaks. The nature of this change depends crucially on the form of

the boundary conditions for c . For symmetric Dirichlet boundary conditions, new peaks arise from the splitting of other peaks, whereas for asymmetric boundary conditions peaks arise near the boundary where $x = 1$. The latter is more consistent with the spatiotemporal patterning observed in the skeletal development in the vertebrate limb.

It should be noted that the patterns arising from model equations (6) and (7), with asymmetric boundary conditions appear in a temporal sequence across the AP axis which is not entirely consistent with that observed in the limb. However, we can modify the model by explicitly including cell differentiation and assuming that differentiation not only depends on the density of undifferentiated cells, but also on an external factor which exists in a gradient across the AP axis. Specifically, the model then becomes

$$\frac{\partial n}{\partial t} = \nabla \cdot (D\nabla n) - \nabla \cdot (n\alpha\nabla c) + s(rn(1-n) - M(x)\Omega(n)) \quad (10)$$

$$\frac{\partial N}{\partial t} = s\Omega(n)M(x) \quad (11)$$

$$\frac{\partial c}{\partial t} = \nabla^2 c + s\left(\frac{n}{n+\gamma} - c\right) \quad (12)$$

where N is the nondimensional density of differentiated cells, $\Omega(n)$ is the function controlling cell differentiation and $M(x)$ is the function which modulates the rate of differentiation across the AP axis. The function $\Omega(n)$ must have the property that it takes very low values for small n and saturates to a high value for large n . Specifically, we consider

$$\Omega(n) = \frac{\beta(n - n_c)^m}{\delta + (n - n_c)^m} \quad (13)$$

where β , n_c , δ , and m are suitably chosen parameters. The modulating function $M(x)$, which models the effect of an external factor which diffuses across the domain from one boundary, is given by

$$M(x) = \frac{\cosh(mx)}{\cosh(20m)} \quad (14)$$

where m is a constant. This form for the function $M(x)$ has been chosen because it represents the steady-state solution of a reaction–diffusion equation where a modulating substance has a fixed concentration (taken to be 1) at $x = 1$ with zero flux at $x = 0$. The only kinetic term is a linear degradation term. This modified model of equations (10)–(12) gives a temporal sequence which is consistent with those observed experimentally in the chick limb (Fig. 12).

The inclusion of cell differentiation alone results in the model having no non-trivial steady state. However, the inclusion of a small amount of dedifferentiation

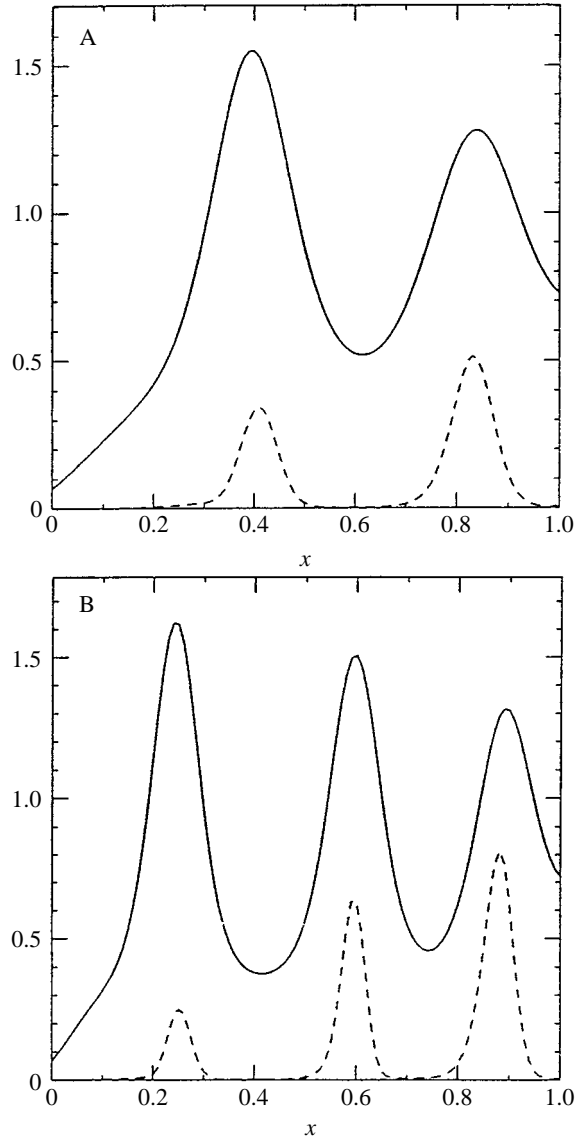


Figure 12. Simulation of the model system (10)–(12) in one spatial dimension for Neumann boundary conditions on n and asymmetric Dirichlet conditions on c , with $c(0) = 0$, $c(1) = 0.45$. Parameter values are $D = 0.25$, $\alpha = 2$, $r = 0.04$, $\gamma = 1$, $M_d = 0.3$, $M_0 = 1$, $\beta = 0.1$, $n_c = 0.3$, $m = 8$; in (a) $s = 400$ and in (b) $s = 1000$. Transient solutions are shown in (a) for $t = 12000$ and in (b) for $t = 6000$. In each case the rightmost aggregate in undifferentiated cells, N , dominates the initial transient solution. The final steady-state patterns (not shown) in (a) have two peaks in N and in (b) have three peaks in N . In both cases the amplitude decreases from left to right. n , —; N - - - [the profiles for c in (a) and (b) are not shown but have two and three peaks, respectively].

leads to steady-state solutions in n , c and N which are qualitatively similar to those for the case of no dedifferentiation. In these cases, the number of peaks, their position and their temporal sequence remain unaltered, but away from the peaks, N eventually tends to zero exponentially.

While pattern is being laid down the limb bud is growing. This can be modeled by taking the scale factor s to be a function of $s(t)$ in equations (10)–(12). Solving the model in this case leads to results that are qualitatively similar to those described.

The above arguments are based on one-dimensional simulations, while the limb is, of course, a three-dimensional structure. To make our model more realistic, we now consider the two-dimensional simulations presented in Section 6. We may think of Type B conditions as corresponding to a two-dimensional cross section of a limb perpendicular to the PD axis, with the source of chemical being at one end of the AP axis. Type A conditions correspond to a cross section perpendicular to the dorso–ventral axis, with the source once more located on one side of the AP axis. Figure 11 shows that, as the domain size increases, there is a transition sequence from one to two to three spots, consistent with the sequence observed along the PD axis, whereas Fig. 9 shows a sequence similar to that observed along the plane of the limb parallel to the dorso–ventral axis. The correct sequence in this case will form only if the aspect ratio is sufficiently small, suggesting that pattern forms in a small strip and not in the full domain. This is consistent with the idea that pattern is laid down in the progress zone.

8. DISCUSSION

In this article we have considered the effect of different boundary conditions on a cell-chemotaxis pattern generator. The introduction of more general boundary conditions leads to significant differences in the spatiotemporal properties of the patterns produced compared with those exhibited under standard Neumann boundary conditions. These are the internalization of the peaks in cell density (that is, no peaks form on the boundary) and the formation of stable patterns with asymmetric peaks. We have chosen to consider the particular case in which the cell density obeys zero flux on the boundary, which is a biologically realistic assumption. Hence, mixed symmetric or asymmetric boundary conditions are introduced by imposing Dirichlet conditions on c .

Imposing homogeneous Dirichlet boundary conditions on chemoattractant concentration c while continuing to use Neumann conditions for cell density n results in peaks occurring within the domain rather than on the boundary. Such boundary conditions eliminate solutions with peaks on the boundary and therefore enhance the robustness of the patterns which do occur. Dillon *et al.* (1993) showed a similar phenomenon in reaction–diffusion models.

Asymmetric fixed boundary conditions on c produce a spatially asymmetric pattern. Such boundary conditions can actually enhance the pattern formation

potential of the cell-chemotactic model. With these boundary conditions peaks do not form simultaneously, but rather form in a sequence which usually starts with the first large peaks forming nearer the boundary where c is lower.

Maini *et al.* (1992) investigated the spatially asymmetric patterns produced by a modified reaction–diffusion system. In their model, two chemicals (morphogens) interacted to give diffusion-driven instability in the standard fashion. The introduction of a third chemical which modulated the diffusion coefficients of the morphogens and had a spatially asymmetric profile resulted in spatially asymmetric steady-state solutions in morphogen concentrations. In their case the introduction of spatially varying diffusion coefficients splits the domain into pattern-forming and nonpattern-forming subdomains. A similar result cannot be obtained for the chemotactic system because a spatial variation in the diffusion or chemotactic coefficients results in one part of the domain being more strongly chemotactic than the other part. The former actually induces gradients in the latter leading to patterns in both parts of the domain. This is an inherent difference between these models.

In the cell-chemotactic model peaks are set up in a specific temporal sequence. In contrast, in the three chemical reaction–diffusion system discussed in Maini *et al.* (1992), the peaks in morphogen concentration form simultaneously. Therefore, the mechanism by which the asymmetry is set up in these two different systems is intrinsically different. In the reaction–diffusion system, a spatially varying diffusion coefficient essentially modifies the underlying pattern formed due to diffusion-driven instability. In the chemotactic system, heterogeneous fixed-boundary conditions in c create gradients in c which implicitly influence the patterning mechanism. Therefore, although the final steady states of the models may look qualitatively similar, the processes that lead to the asymmetry are essentially very different.

ACKNOWLEDGEMENTS

This work was supported by an Australian Research Council Small Grant (to MRM). PKM would like to thank the School of Mathematics and Statistics, University of Sydney, for their hospitality. KJP was supported by an EPSRC Earmarked Studentship in Mathematical Biology.

APPENDIX

A.1. Analytical Determination of Aspect Ratio. We begin our determination of the aspect ratio through consideration of the more standard case, in which the boundary conditions for both the cell density and chemical concentration are zero flux everywhere. A standard linearization of the model system (6)–(7) about the

homogeneous steady state $(1, c^s)$, yields the following linearized set of equations:

$$\frac{\partial u}{\partial t} = D\nabla^2 u - \alpha\nabla^2 v - sru \quad (15)$$

$$\frac{\partial v}{\partial t} = \nabla^2 v + s\left(\frac{\gamma}{(\gamma+1)^2}u - v\right) \quad (16)$$

where $u = n - 1$, $v = c - c^s$. We seek solutions to the linearized system of the form:

$$\underline{w} \sim \exp(i\underline{k} \cdot \underline{x} + \lambda t), \quad (17)$$

subject to the boundary conditions, where $\underline{w} = (u, v)^T$ and $\underline{x} = (x, y)^T$.

The dispersion relation is given by:

$$\lambda^2 + a(k^2)\lambda + b(k^2) = 0 \quad (18)$$

where

$$a(k^2) = (D+1)k^2 + s(r+1) \quad (19)$$

$$b(k^2) = Dk^4 + \left(Ds + rs - \frac{s\gamma\alpha}{(1+\gamma)^2}\right)k^2 + s^2r \quad (20)$$

Heterogeneous solutions will develop only when the real part of λ becomes positive for admissible values of k^2 . For zero-flux boundary conditions on the domain $[0, 1] \times [0, W]$, such k^2 are of the form

$$k^2 = \pi^2 \left(p^2 + \frac{q^2}{W^2}\right) \quad (21)$$

where $p, q \in \mathbb{N}$.

We know that $a(k^2) > 0$ for all $k^2 > 0$, and so heterogeneous patterns are possible only if there exists a range of k^2 for which $b(k^2) < 0$.

The conditions are thus given by:

$$\frac{s\gamma\alpha}{(1+\gamma)^2} > (D+r)s \quad (22)$$

$$\left(\frac{s\gamma\alpha}{(1+\gamma)^2} - (D+r)s\right)^2 > 4Ds^2r \quad (23)$$

When these conditions are satisfied, we obtain a range of $k^2 \in \mathbb{R}^+$ for which the steady state is unstable in the linearized system. When a finite domain is

considered, however, the only heterogeneous solutions that grow are those that satisfy the boundary conditions. This equates to requiring the set given by:

$$\left\{ (p, q) \in \mathbb{N}^2 : \pi^2 \left(p^2 + \frac{q^2}{W^2} \right) \in (k_l^2, k_u^2) \right\} \quad (24)$$

to be nonempty, where k_l and k_u are, respectively, the lower and upper intercepts of the dispersion curve with the k^2 axis.

The linearized solutions give us an idea to the type of solutions we may expect to the system for a given set of parameters. We therefore fix all model parameters apart from W and consider the range of unstable modes when W is small.

The function given by $\frac{q^2}{W^2}$ tends to infinity as W tends to zero and thus for sufficiently small W (and $q > 0$),

$$\pi^2 \frac{q^2}{W^2} > k_u^2 \quad (25)$$

In this case, the only unstable modes are those for which $q = 0$. Obviously,

$$\pi^2 \frac{q^2}{W^2} < \pi^2 p^2 + \pi^2 \frac{q^2}{W^2}, \quad (26)$$

and so the first mode that becomes unstable as W is increased, for which $q \neq 0$ will be the $(0, 1)$ mode.

Thus to find the minimum aspect ratio, we determine the size of W for which the $(0, 1)$ mode becomes unstable. The problem effectively becomes a one-dimensional problem. The critical length for stripe solutions to the zero-flux problem is given by

$$W_c = \frac{\pi}{k_u} \quad (27)$$

where k_u is given by

$$\begin{aligned} k_u^2 = & \frac{1}{2D} \left(\left(\frac{s\gamma\alpha}{(1+\gamma)^2} - (D+r)s \right) \right. \\ & \left. + \sqrt{\left(\left(\frac{s\gamma\alpha}{(1+\gamma)^2} - (D+r)s \right)^2 - 4Ds^2r \right)} \right) \end{aligned} \quad (28)$$

Using the parameters in the simulations presented in this paper, the critical length is determined by

$$W_c = \frac{5\sqrt{2}\pi}{\sqrt{s(21 + \sqrt{41})}} \quad (29)$$

Table A1. Numerical and analytical comparison of maximal domain width for stripe solutions. Numerical results are to two decimal place accuracy and given are the smallest W_c for which stripes break down in two dimensions.

s	Analytical W_c	Numerical W_c
300	0.245	—
400	0.212	0.21
900	0.141	0.14
3000	0.078	0.08

We have thus shown how the linear analysis can predict the onset of patterning for the model with zero flux at the boundary.

In our system, however, only the cell population has zero-flux conditions everywhere. The chemical concentration is bounded on two sides of the domain with asymmetric Dirichlet conditions, and zero flux at the other boundaries. The effect of increasing s , however, is to increase the domain size and, effectively, increase the length of domain between the Dirichlet boundaries. We can thus argue that, as s is increased, the influence of the boundaries on the patterning at the center of the domain weakens, and so the system can be approximated by the one-dimensional problem of searching for the point of instability of the (0, 1) mode.

This hypothesis is strongly supported by the results of numerical simulations. A comparison between critical aspect ratios predicted by the above analysis and the numerically determined values is shown in Table A1.

The analytical prediction apparently breaks down near $s = 300$. We have analyzed aspect ratios down to 0.5, (corresponding to $W_c = 2$), with no apparent breakdown of the stripe solutions. This suggests that the boundary conditions are strong enough to influence the entire domain.

REFERENCES

- Bard, J. and I. Lauder (1974). How well does Turing's theory of morphogenesis work? *J. Theor. Biol.* **45**, 501–531.
- Brümmer, F., G. Zempel, P. Buhle, J. C. Stein and D. F. Hulser (1991). Retinoic acid modulates gap junction permeability: A comparative study of dye spreading and ionic coupling in cultured cells. *Exp. Cell. Res.* **196**, 158–163.
- Chaplain, M. A. J. and A. M. Stuart (1993). A model mechanism for the chemotactic response of endothelial cells to tumour angiogenesis factor. *IMA J. Math. Appl. Med. Biol.* **10**, 149–168.
- Dillon, R., P. K. Maini, and H. G. Othmer (1993). Pattern formation in generalised Turing systems: I. Steady-state patterns in systems with mixed boundary conditions. *J. Math. Biol.* **32**, 345–393.
- Ford, R. M. and D. A. Lauffenberger (1991). Analysis of chemotactic bacterial distributions in population migration assays using a mathematical model applicable to steep or shallow attractant gradients. *Bull. Math. Biol.* **53**, 721–749.
- Grindrod, P., S. Sinha and J. D. Murray (1989). Steady state spatial patterns in a cell-chemotaxis model. *IMA J. Math. Appl. Med. & Biol.* **6**, 69–79.
- Gueron, S. and N. Liron (1989). A model of herd grazing as a travelling wave, chemotaxis and stability. *J. Math. Biol.* **27**, 595–606.

- Höfer, T., J. A. Sherratt and P. K. Maini (1995a). Dictyostelium discoideum: Cellular self-organisation in an excitable medium. *Proc. Roy. Soc. Lond.* **B259**, 249-257.
- Höfer, T., J. A. Sherratt and P. K. Maini (1995b). Cellular pattern formation during *Dictyostelium* aggregation. *Physica* **D85**, 425-444.
- Hunding, A. and M. Brøns (1990). Bifurcation in a spherical reaction diffusion system with imposed gradient. *Physica* **D44**, 285-302.
- Keller, E. F. and L. A. Segel (1970). Initiation of slime mold aggregation viewed as an instability. *J. Theor. Biol.* **26**, 399-415.
- Keller, E. F. and L. A. Segel (1971). Travelling bands of bacteria: a theoretical analysis. *J. Theor. Biol.* **30**, 235-248.
- Kulesa, P., G. C. Cruywagen, S. R. Lubkin, P. K. Maini, J. S. Sneyd and J. D. Murray (1995). Modelling spatial patterning of the primordia in the lower jaw of *Alligator mississippiensis*. *J. Biol. Syst.* **3**, 975-985.
- Lapidus, I. R. and R. Schiller (1976). A model for the chemotactic response of a bacterial population. *Biophys. J.* **16**, 779-789.
- Maini, P. K., M. R. Myerscough, K. H. Winters and J. D. Murray (1991). Bifurcating spatially heterogeneous solutions in a chemotaxis model for biological pattern formation. *Bull. Math. Biol.* **53**, 701-719.
- Maini, P. K. (1994). Coupled models for spatial organization in development. *Ber. Bunsenges. Phys. Chem.* **98**, 1172-1175.
- Maini, P. K. and M. Solursh (1991). Cellular mechanisms of pattern formation in the developing limb. *Int. Rev. Cytol.* **129**, 91-133.
- Maini, P. K., D. Benson and J. A. Sherratt (1992). Pattern formation in reaction diffusion models with spatially inhomogeneous diffusion coefficients. *IMA J. Math. Appl. Med. & Biol.* **9**, 197-213.
- Murray, J. D. (1989). *Mathematical Biology*, New York: Springer-Verlag
- Murray, J. D., D. C. Deeming and M. J. W. Ferguson (1990). Size dependent pigmentation pattern formation in embryos of *Alligator mississippiensis*: Time of initiation of pattern formation mechanism. *Proc. Roy. Soc. (London)* **B239**, 279-293.
- Murray, J. D. and M. R. Myerscough (1991). Pigmentation pattern formation on snakes. *J. Theor. Biol.* **149**, 339-360.
- Myerscough, M. R. (1988). *A chemotactic model for biological pattern formation*. DPhil thesis, Corpus Christi College, Oxford, U.K.
- Myerscough, M. R. and J. D. Murray (1992). Analysis of propagating pattern in a chemotaxis system. *Bull. Math. Biol.* **54**, 77-94.
- Nagorcka, B. N. (1989). Wavelike isomorphic prepatterning in development. *J. Theor. Biol.* **137**, 127-162.
- Newman, S. A. and H. L. Frisch (1979). Dynamics of skeletal pattern formation in developing chick limb. *Science* **205**, 662-668.
- Oster, G. F., J. D. Murray and A. K. Harris (1983). Mechanical aspects of mesenchymal morphogenesis. *J. Embryol. Exp. Morphol.* **78**, 83-125.
- Oster, G. F., N. Shubin, J. D. Murray and P. Alberch (1988). Evolution and morphogenetic rules. The shape of the vertebrate limb in ontogeny and phylogeny. *Evolution* **45**, 862-884.
- Othmer, H. G. (1986). On the Newman-Frisch model of limb chondrogenesis. *J. Theor. Biol.* **121**, 505-508.
- Othmer, H. G. and A. Stevens (1997). Aggregation, blow-up and collapse: the ABCs of taxis in reinforced random walks. *SIAM J. Appl. Math* **57**, 1044-1081.

- Sherratt, J. A., E. H. Sage and J. D. Murray (1993). Chemical control of eucaryotic cell movement: a new model. *J. Theor. Biol.* **162**, 23–40.
- Turing, A. (1952). The chemical basis of morphogenesis. *Phil. Trans. Roy. Soc. Lond.* **B237**, 37–72.
- Winters, K. H. (1985). *Entwife User Manual (Release 1)*, Theoretical Physics Division AERE, Harwell, Oxfordshire, U.K.
- Wolpert, L. (1969). Positional information and the spatial pattern of cellular differentiation. *J. Theor. Biol.* **25**, 1–47.

Received 13 August 1995 and accepted 12 June 1997